Cellulose (2021) 28:8493–8508
https://doi.org/10.1007/s10570-021-03995-4

ORIGINAL RESEARCH

Mechano-chemically activated fly-ash and sisal fiber reinforced PP hybrid composite with enhanced mechanical properties

Atul Kumar Maurya · Rupam Gogoi · Gaurav Manik

Received: 19 January 2021 / Accepted: 10 June 2021 / Published online: 22 June 2021

Abstract This study explores the hybridizing effect of mechano-chemical activated fly-ash (FA) in polypropylene (PP) composites reinforced with sisal fibers. Activation and resistance against agglomeration of FA has been achieved by modifying it with 2, 4, and 6 wt.% of the cetyltrimethylammonium bromide (C-tab). FA activation with C-tab and particle size reduction to nano-level (< 1 μm) have been appropriately achieved with a planetary ball milling and the same has been confirmed from the dynamic light scattering technique. The hybrid composite containing 25 wt.% of sisal fiber and 5 wt.% of (6 wt.% C-tab) treated FA shows much improved tensile (40.12 MPa), flexural (53.27 MPa), and impact strengths (0.75 kJ/m^2) than that of virgin PP and its 30 wt.% sisal fiber composites. This increase in tensile and flexural strength was 30.54% and 48% higher than neat PP. Maximum notched impact strength of 0.80 kJ/m^2 have been reported by hybrid composite containing FA treated with 2 wt.% of the C-tab. Micromechanical modelling using a combination of rule of mixture and inverse rule of mixture separately with Halpin–Tsai predicted a value close to the experimental Young's modulus. DSC studies showed an increment in the composite's crystallinity upon fiber addition. Morphological analysis of the hybrid composite revealed good wettability of reinforcing fiber and FA within the matrix, whereas TGA showed an improved thermal stability of the composites.

Supplementary information The online version contains supplementary material available at https://doi.org/10.1007/s10570-021-03995-4.

A. K. Maurya · R. Gogoi · G. Manik (✉)
Department of Polymer and Process Engineering, Indian Institute of Technology Roorkee, Saharanpur Campus, Paper Mill Road, Saharanpur, Uttar Pradesh 247001, India
e-mail: manikfpt@iitr.ac.in; gaurav.manik@pe.iitr.ac.in; gauravmanik3m@gmail.com

A. K. Maurya
e-mail: amaurya@pe.iitr.ac.in

Graphic abstract

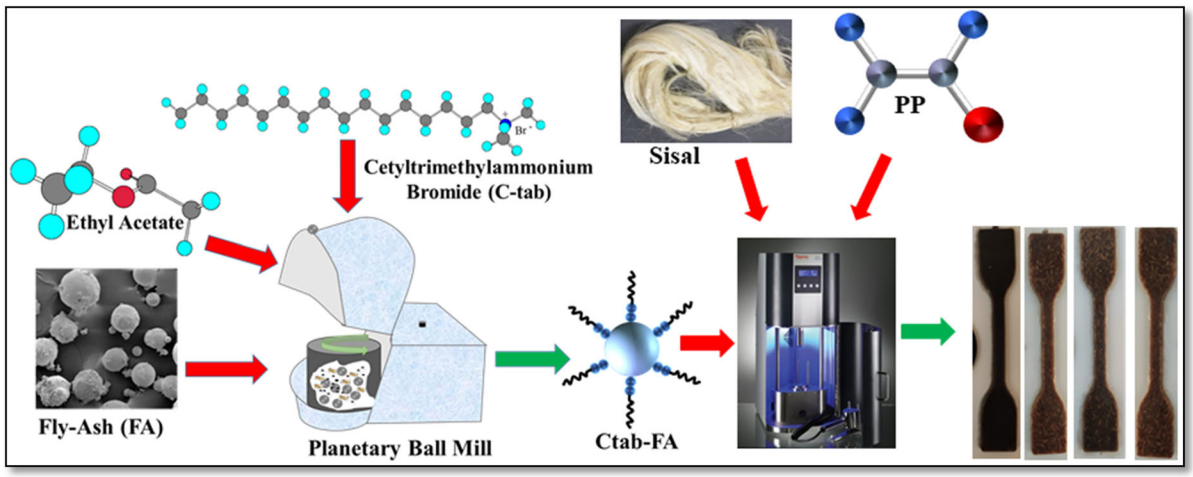

Keywords Hybrid composites · Natural fiber · Fly-ash · C-tab · Micromechanical modelling · Sustainable development

Introduction

Ligno-cellulosic natural fibers have been drawing the attention of researchers worldwide for many decades as suitable substitutes for synthetic fibers due to their eco-friendly, techno-economical, and renewable advantages (Sanjay et al. 2018; Senthilkumar et al. 2018). Low density, high specific mechanical properties, and desirable biodegradability of natural fibers make their use beneficial over that of synthetic fibers (AL-Oqla 2021). Cellulosic fibers such as kenaf, ramie, flax, hemp, and sisal have been already lately proposed and employed in various applications (Faruk et al. 2012; Sanjay et al. 2016). For instance, the use of flax fiber over carbon fiber for making seats of formula one racing cars provides a sustainable technology and reduces carbon footprint as opposed to their synthetic counterparts (Surani 2021). Another such robust, durable, and strong natural fiber with resistance against moisture and salt water is sisal fiber (Naveen et al. 2018). Sisal fiber has specific strength and modulus comparable to that of glass fiber which make them ideal reinforcing agent. Various applications of composites reinforced with sisal fiber includes, but not limited to, automobile parts, interior paneling of aircraft, door panels, hat racks, interior engine covers, and floor paneling (Naveen et al. 2018; Senthilkumar et al. 2018). The evaluation, methodologies, and performance of some other bio-based composites were established recently (Black et al. 2011; Gogoi et al. 2019a; Maurya et al. 2021). However, for a successful design of natural fiber reinforced composites, they need to be stable under many harsh environmental conditions affected by thermal, wet, mechanical, and high friction, and meet the performance or regulatory criteria (Abral et al. 2014; Abdal-Hay et al. 2012; Gogoi et al. 2019b). In different circumstances, a proper combination of natural fiber and other inorganic ingredients may improve the thermal stability, moisture mitigation and mechanical performance of the composites (Maurya et al. 2021).

Polymers are non-polar and hydrophobic in nature, whereas natural fibers are hydrophilic. Interfacial interactions or adhesion decide the load transfer from matrix to reinforcements and affect the mechanical and other physical and chemical properties of the composites, including moisture absorption (Sanjay and Siengchin 2019; AL-Oqla and Hayajneh 2020). Many techniques such as chemical/physical/biological treatment of fiber (Hamidon et al. 2019), use of suitable coupling agent (Kumar et al. 2017), or a combination of both of these methods (Maurya et al. 2021) have already been reported earlier for improving interfacial adhesion. Most optimized interfacial

adhesion technique reported so far was use of combined alkali and silane treatment along with a suitable coupling agent (Panaitescu et al. 2019; Maurya et al. 2021). Although reinforcement with natural fiber and its formation of strong interfacial bonds with polymer matrix reported improved tensile and flexural properties but, in parallel, inclusion of strong and stiff fiber also decreases the impact strength of matrix and increases its moisture absorption (Panaitescu et al. 2019; Maurya et al. 2021). A possible approach to overcome the above issue of low impact strength is to blend the base polymer matrix with toughening agents like SEBS, EPR, and SBS (Liu et al. 2008; Panaitescu et al. 2019; Maurya et al. 2021). Likewise, SEBS (Panaitescu et al. 2019) and SEBS/SEBS-g-MA in our previous work (Maurya et al. 2021) were used for improving the impact properties of the natural fiber reinforced polymer composites. It was expected that the rubbery nature of these toughening agents must have improved the impact strength by making crosslinks among polymer network. FA, waste from the thermal power plant, could be a possible answer for maintaining these properties altogether. FA, which contains many hazardous and heavy metals like Pb, As, Cr, etc., is also harmful for aquatic life and the human environment. In general, the chemical composition of FA consists of more than 60% of aluminum and silicon dioxide (SiO_2 and Al_2O_3). The surface treatment of FA using suitable silane/surfactant/long-chain fatty acids have shown positive results in enhancing the interfacial adhesion with polymer matrix and also showed improvement in impact strength (Joseph et al. 2011; Sengupta et al. 2013b). In this direction, Joseph et al. (Joseph et al. 2011) and Sengupta et al. (Sengupta et al. 2011) used silane and furfuryl palmitate/palmitic acid for surface treatment of FA, respectively, and reported improved impact strength of the composite. Hence, use of FA as a filler with improved mechanical properties would be the right approach in handling hazardous waste like FA and creating composites through a greener and sustainable approach. However, from our previous study it was clear that use of FA with particle size $\sim$ 2 μm as filler, with natural fiber reinforcement for base matrix pre-optimized with SEBS and MA-g-SEBS, showed improved impact strength and moisture mitigation. There was, however, unnoticeable improvement in tensile or flexural properties (Maurya et al. 2021). It was also concluded that all the hybrid composites exhibited impact strength higher than that of PP, base matrix and composites consisting of only sisal fiber. Among all the investigated formulations, only one hybrid composite containing 25 wt.% of sisal fiber and 5 wt.% of silane treated fly ash reported slightly higher tensile and flexural properties compared to PP. The current study is the extended version of the previous work.

The primary objective of the current study is to fabricate composites having high impact, tensile, flexural strength and thermal stability by using a suitable combination of waste (FA) and bio-reinforcements (sisal fiber) in the polymer. It was earlier reported that use of nano/inorganic fillers with short fibers decreases the interfacial gap between reinforcement and matrix (Khandelwal and Rhee 2020; Sumesh et al. 2020) resulting in increased load bearing capacity of the composites. The same positive hybridization effect on mechanical performance was observed and reported for hybrids composites consisting of sisal and pineapple fiber, inorganic filler and basalt fiber earlier (Khandelwal and Rhee 2020; Sumesh et al. 2020). Motivated by the aforementioned approaches, the current study uses 5 wt.% FA filled and 25 wt.% short sisal fiber reinforced PP as the hybrid formulation for investigating various properties. Fibers were given a combined treatment of alkaline and silane (APTES) for optimum properties. In previous reports, silane treatment and particle size of $\sim$ 2 μm for the FA were not effective parameters in increasing tensile and flexural properties. Hence, in the present study the silane treatment was replaced with cationic surfactant C-tab in varying wt.% (2–6%) along with sub-micron or nanostructured particle size of FA. The size reduction of FA fillers was achieved by planetary ball milling in ethyl acetate medium. C-tab has been earlier reported as a good dispersing agent for the microcrystalline cellulose (Filho et al. 2021), and hence, it was expected that it would reduce the agglomeration of the FA within the composites and during processing as well. It was also expected that the nanostructure of the FA would provide greater surface area for interaction with the base matrix. To the best of our information, none of the literature reported the use of high energy ball milled nano structured FA (thermal power plant waste) as a filler with natural fiber PP composites, and demonstrated apparent benefits.

Additionally, inorganic or nanofiller/short fiber generally reduces the impact strength of the

composites (Gogoi et al. 2019c; Panaitescu et al. 2019). To counter this effect, an impact-modified PP blend was used as a base matrix. The base matrix was selected from a pre-optimized blend of PP, SEBS, and maleic anhydride-grafted-SEBS (Maurya et al. 2021). Alkali-silane treated sisal fiber and C-tab treated FA were used in combination and separately to fabricate different composites and their hybrids. Different mechanical, thermal, and morphological properties were estimated for the composites and reported here. In addition, micromechanical modeling of the hybrid composites was done to model and simulate their tensile modulus using various established empirical relations, and compare these with experimental results.

Micromechanical modelling

To predict the Young's modulus of the composite various empirical and semi-empirical equations have been developed by scientists using the polymers matrix and its properties of constituents. Two approaches based on, (1) Mechanics of materials and (2) Elasticity were adopted previously for micromechanical analysis. However, the current study uses an elasticity based rigorous that covers at least three aspects: bounding principles, exact solutions, and approximate solutions (Gogoi et al. 2019c). Gogoi et al. (Gogoi et al. 2019c) used particulate and matrix collectively assumed as the first component, reinforcing fiber as the second component and evaluated the modulus of the hybrid composite consisting of particulate and fiber-filled composite. Various recognizable models and equations for particulate and fiber-reinforced composites have been given below and a mixture of these models have been used in this investigation to calculate hybrid composites modulus.

The following rules have been used to estimate the composite modulus.

Rule of mixture (Parallel model) and inverse rule of mixture (Series model)

(i) Rule of mixture:

$$E_c = E_m V_m + E_r V_r \tag{1}$$

(ii) Inverse rule of mixture:

$$E_c = \frac{E_r E_m}{E_m V_r + E_r V_m} \tag{2}$$

In the above equations,

$$V_r = \frac{\rho_m \omega_r}{\rho_m \omega_r + \rho_r \omega_m} \tag{3}$$

$$V_m = 1 - V_r \tag{4}$$

where E_c, E_m and E_r stand for the moduli of composite material, matrix and reinforcement (particle/fiber), respectively. Likewise, V_r, ρ_m, ω_r, ρ_r, ω_m, and V_m stands for the volume fractions of the reinforcement, density of matrix, weight fraction of the reinforcement, density of the reinforcement, weight fraction of the matrix, and volume fraction of the matrix repectively.

(iii) Halpin–Tsai model:

$$E_L = E_m \left[\frac{1 + \xi \left(\frac{l_r}{d_r} \right) \eta_L V_r}{1 - \eta_L V_r} \right] \tag{5}$$

$$E_T = E_m \left[\frac{1 + \xi \eta_T V_r}{1 - \eta_T V_r} \right] \tag{6}$$

where η_L and η_T are functions of the ratio of the fiber and matrix moduli, and the reinforcement factor ξ, these may be calculated using following equation

$$\eta_L = \frac{\left(\frac{E_r}{E_m} \right) - 1}{\left(\frac{E_r}{E_m} \right) + \xi \left(\frac{l_r}{d_r} \right)} \tag{7}$$

$$\eta_T = \frac{\left(\frac{E_r}{E_m} \right) - 1}{\left(\frac{E_r}{E_m} \right) + \xi} \tag{8}$$

Reinforcing factor ξ is dependent on the fiber geometry, packing geometry and loading conditions. The value of ξ may vary from 0 to ∞. ξ =2 has been taken for current study. An approximate estimation of modulus can be predicted using Halpin-Tsai model

$$E_c^{random} = \frac{3}{8}E_L + \frac{5}{8}E_T \tag{9}$$

where E_c^{random} denotes the tensile modulus of randomly oriented short fiber reinforced polymer composite.

(iv) Ishai and Cohen equation.

This model offers an approximate estimate of upper and lower modulus of the composite using:

$$\frac{E_c^{upper}}{E_m} = 1 + \frac{1 + (\delta - 1)V_r^{\frac{2}{3}}}{1 + (\delta - 1)\left(V_r^{\frac{2}{3}} - V_r\right)} \tag{10}$$

$$\frac{E_c^{lower}}{E_m} = 1 + \frac{V_r}{\frac{\delta}{(\delta - 1)} - V_r^{\frac{1}{3}}} \tag{11}$$

where $\delta = \frac{E_r}{E_m}$.

(v) Einstein's equation

$$\frac{E_c}{E_m} = 1 + 2.5V_r \tag{12}$$

(vi) Guth

$$\frac{E_c}{E_m} = 1 + 2.5V_r + 14.1V_r^2 \tag{13}$$

(vii) Mooney

$$\frac{E_c}{E_m} = \frac{exp(2.5V_r)}{1 - sV_r} \tag{14}$$

Here, ratio between apparent volume to true volume filled with particles is the crowding factor denoted by s. Value of s can be varied from 1 to 2. In this direction, based on assumption of perfect filler-matrix interaction in particulate composite Counto proposed another model given by.

(viii) Counto

$$\frac{1}{E_c} = \frac{1 - V_r^{\frac{1}{2}}}{E_m} + \frac{1}{\frac{\left(1 - V_r^{\frac{1}{2}}\right)}{V_r^{\frac{1}{2}}E_m} + E_r} \tag{15}$$

In the present work, the hybrid composite modulus has been predicted using various numerical models for particulate and short fiber-reinforced composite. The experimental results have been compared and analyzed to check their applicability.

The hybrid composite modulus has been evaluated using a combination of various empirical and semi-empirical formulas based on short fiber and particle reinforced composite. For simplicity, FA filled composite has been considered as the effective matrix for hybrid composite to reinforce short natural fiber. A similar approach was used for HGM filled carbon fiber reinforced PP hybrid composite by Gogoi et al. (Gogoi et al. 2019c). The tensile modulus of the hybrid composites in the present study has been evaluated using the empirical models. The following parameters were considered for the entire calculation. For *eff*-BM V_{bm} = 0.96 (volume fraction of BM) and V_{fa} = 0.04. For hybrid composite, $V_{eff\text{-}BM}$ = 0.66, V_{ssl} = 0.34 (volume fraction of sisal fiber), V_{fa} = 0.04 (volume fraction of FA), E_{bm} = 730 MPa (tensile modulus of BM), E_{ssl} = 3800 MPa (tensile modulus of SSL), l_f = 6 mm (fiber length), d_f = 185.17 µm (fiber diameter), and E_{fa} = 1881 MPa (tensile modulus of FA). BM filled with 5 wt.% FA was chosen as the effective matrix (*eff*-BM) for the theoretical analysis. The effective tensile modulus of this particulate composite, $E_{eff\text{-}BM}$. Density of the respective system was evaluated using Equation S1 and the corresponding values has been listed in Table S1.

Materials

PP (Repol H110MA) was procured from Reliance industries and possessed MFI of 11 g/min at 230 °C with a weight of 2.16 kg and and density of 0.908 g/cm^3, respectively. DZBH new materials, China supplied MA-g-SEBS (Beiwa® 901) having 30% styrene content. It has a density of 0.96 gm/cm^3 and a MFI of 43 g/10 min measured at 200 °C with a weight of 5 kg. SEBS (Kraton G1651) H Linear triblock copolymer was purchased from Kraton Polymers (USA) with a specific gravity of 0.91 g/cm^3, tensile strength of 27.6 MPa, and a styrene/rubber ratio of 33–67. Cetyltrymethylammonium bromide (C-tab) has been purchased from Sisco Research Laboratories (SRL) with a pH value of 5–7 and melting point of 249–253 °C.

Preparing base matrix

An optimized blend of PP, SEBS, and MA-g-SEBS was first prepared as a base matrix for the fabrication of composites. Improved impact, tensile, and interfacial adhesion was observed for the base matrix when used for fiber or FA filled composites and the same has been already reported in our previous study (Maurya et al. 2021). The optimized blend used in the present study consists of 85 wt.% PP, 10 wt.% SEBS and 5 wt.% of SEBS-g-MA and was termed as the base matrix (BM). Hakke Rheomix QC Lab mixer supplied by ThermoFisher SCIENTIFIC was operated for around 15–20 min at 10–50 rpm to mix different phases of all the components to form the BM. The compounding temperature was maintained between 185 and 190 °C.

Fly-ash treatment

FA (Fillit^{TM} 500 s) was obtained from Petra build care products, India. It had a particle size of 5–500 µm, density around 0.80–0.83 g/cm^3, and moisture content of less than 0.5%. The activation of FA particle with C-tab has been achieved by using high energy planetary ball milling (Make: Retsch Germany) in ethylene acetate and 250 ml tungsten carbide medium for 8 h at 250 rpm. 10 mm diameter tungsten carbide balls in 10:1 ratio was used for milling the FA. To avoid heat build-up during the ball milling, a break time of 60 s was given at an interval of 30 min for every 2 h of continuous milling. During this process, the particle size of FA was reduced to ∼ 900 nm which is the most probable size measured using DLS and also confirmed by FESEM. The DLS measurement is shown in Figure S1.

Alkali-silane treatment of reinforcing sisal fiber

The benefit of a small lignin content in increasing the reinforcement and compatibilizing effect has been reported by many researchers in the past. Moreover, a complete bleach of the lignin from the fiber surface may put down the interaction between π electrons of SEBS containing an aromatic moiety and lignin (Gadioli and Morais et al. 2014). Partial treatment with alkali increases surface roughness, removes a part of lignin, wax, and pectin, etc. Hence, a limited treatment of SSL fibers was carried out at 80 °C using 1 wt.% of NaOH solution. Prior to their treatment, the fibers were properly washed and dried. After NaOH treatment, SSL fibers were rewashed multiple times until a pH of 7 was obtained. Excess NaOH on the fiber surface was neutralized by washing it with 1 wt.% of acetic acid solution (Fig. 1).

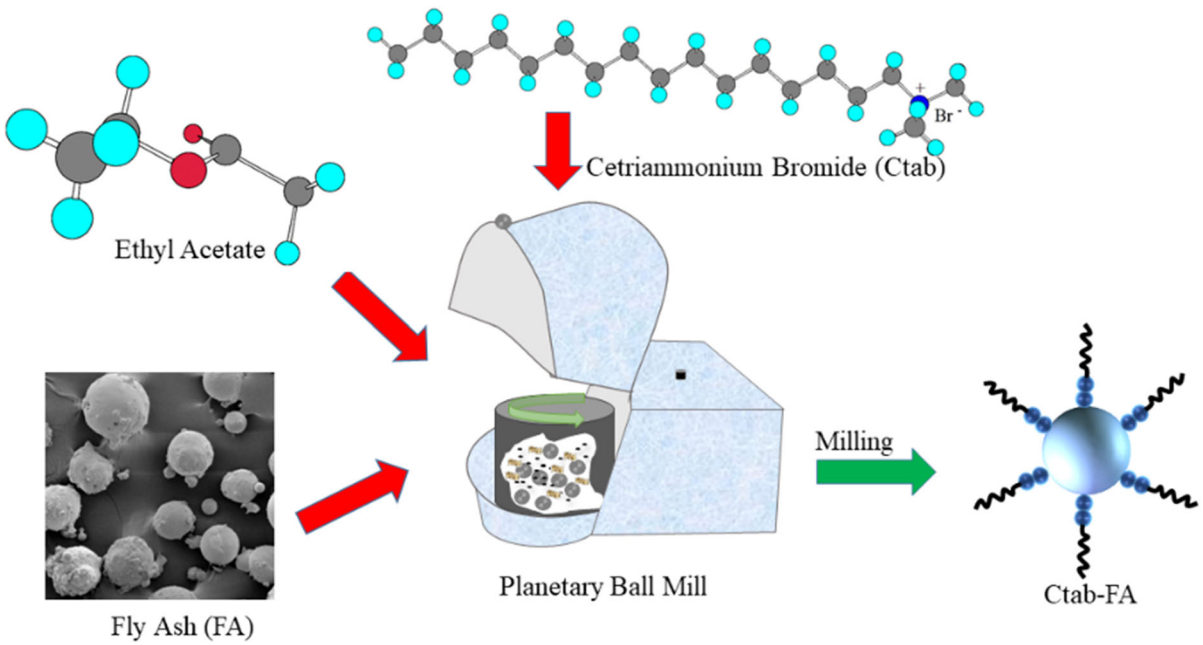

Fig. 1 Illustration of high energy ball milling of FA in a planetary ball mill

For drying, NaOH-treated fiber was kept at room temperature for one week. Before, silane treatment SSL fibers were de-moisturized in a microwave oven for 8 h at 60 °C. Considering the silane treatment, a 90:10 ethyl alcohol and water solution was prepared followed by the addition of 2 wt.% 3-aminopropyl triethoxysilane (APTES). Alkali treated SSL fiber has been added to this solution for alkali-silane treated SSL fiber at 60 °C. Treatment of SSL fiber with NaOH skims a small part of lignin and surface impurities. Partial removal of lignin increases the surface roughness and makes –OH groups available for further interaction with silane group which ultimately enhances surface coating (Koohestani et al. 2019)(Panaitescu et al. 2019). Alkali-silane coated SSL fiber is favorable for good dispersion and interfacial interaction with polymer matrix (Panaitescu et al. 2019). Such treated SSL fibers of 6 mm length were used for the composite fabrications.

Sample preparation

Prior to the composite fabrication, all the materials such as PP, MA-g-SEBS, SEBS, SSL fiber, and FA were dried in an air and vacuum oven at 60 °C for 12 h and 3 h, respectively. The BM was prepared as mentioned in section"Preparing base matrix". Nomenclature of all the composites assigned here (6FA/BM and 2FA/SSL/BM, 4FA/SSL/BM, and 6FA/SSL/BM) and their corresponding compositions have been shown in Table 1. The FA proportion was selected based on previous articles (Joseph et al. 2011) (Maurya et al. 2021), which suggests that 5 wt.% FA is optimum for the composites.. Initially all the ingredients of the composites were properly mixed in a Haake Rheomix. Granules or chunks from the Rheomix were melted and extruded in a micro compounder HAAKE^{TM} MiniCTW maintained at 190 °C and 50 rpm. The composite melt from the micro compounder was subjected to injection in the HAAKE^{TM} Minijet II (set at 180 °C) to form various composites samples for testing.

Table 1 List of compositions used for blends and composites

Sample	C-tab wt.%	Weight percentage (wt.%)		
		BM	FA	SSL
PP	NA	NA	NA	NA
BM	NA	NA	NA	NA
6FA/BM	6	95	5	0
2FA/SSL/BM	2	70	5	25
4FA/SSL/BM	4	70	5	25
6FA/SSL/BM	6	70	5	25

6FA/BM is the 6 wt.% C-tab treated FA incorporated in a 5:95 ratio to the base matrix (BM). Also, prefix 2, 4 and 6 represent wt.% C-tab treatment of the FA in hybrid composites fabricated by reinforcing 5 wt.% of FA and 25 wt.% of sisal fiber (SSL) in the base matrix (BM)

Testing and characterization

Tensile properties

ISO-527–2 standard was followed for testing the tensile properties of all the samples on UTM (Make: INSTRON 5KN Model 3365). Values reported for tensile data are an average of 5 samples from each category tested with a crosshead speed of 15 mm/min at ambient temperature.

Flexural properties

A rectangular sample was used for testing flexural properties of all the samples as per ISO 178:2019 standard on UTM (Make: INSTRON 5KN Model 3365). An average data of 5 samples from each specimen was recorded and reported for a 2 mm/min crosshead speed.

Impact properties

Impact properties of all the samples were studied using Izod impact testing with a notch (0.25 ± 0.05 mm, 45°) following ISO 180 standard on Impact 104 (Make: Tinius Olsen). Data reported here are an average value of 5 samples from each category.

Morphological analysis

Morphology of various samples were analyzed using FE-SEM (Make: Mira3 Tescan). Prior to the test, samples were gold coated and fasten-on aluminum stub while the test was conducted at an acceleration voltage of 5 kV.

Differential scanning calorimetry (DSC)

ASTM D3418-15 was followed on TA instrument (Discovery series DSC 25) for the thermal characterization. About 5 to 10 mg of samples were placed in an aluminium crucible and exposed to heating and cooling cycles (minimum 2) within a temperature range of −60 °C to 250 °C with 10 °C/min heating rate and 5 °C/min cooling rate under a nitrogen atmosphere. Each sample was heated in the first cycle from ambient temperature to 250 °C. To clear any thermal history an isothermal step of 2 min was given to the samples. The second (cooling) and third (heating) cycle involves cooling down from 260 °C to −60 °C and then again heating from −60 °C to 250 °C, respectively. The crystallization temperature and melting temperature/heat of enthalpy were recorded from cooling cycle (second cycle) and second heating (third cycle), respectively. The following formula was used to determine the percent crystallinity of the composites and pristine samples.

$$\%X_c = \frac{\Delta H}{\Delta H^*} \times 100 \quad (16)$$

where ΔH and ΔH^* are the melting enthalpies of samples and 100% crystalline PP, respectively. The value of ΔH^* has been selected 209 J/g for this experiment reported, in literature (Gogoi et al. 2019a).

Thermal degradation

To analyze thermal stability and thermal degradation behavior of the various samples, ASTM E1131-08 (2014) standard was followed. In the Extar TG/DTA instrument, approximately 10 mg samples of each category were heated separately from room temperature (23 °C) to 800 °C at a heating rate of 10 °C/min in a nitrogen (N_2) environment.

Results and discussion

Tensile strength

Various studies have already reported that reinforcing 5 wt.% of FA with natural fiber in polymer composites gives optimum mechanical properties (Joseph et al. 2011). Composite 6FA/BM has been supported with 5 wt.% FA (6% C-tab treated high energy ball milled) using BM as the base matrix. It was expected that hybridizing the composite 6FA/BM with natural fiber will increase the mechanical properties of the hybrid composites. As seen in Fig. 2, the tensile strength and modulus of all the hybrid composites (2FA/SSL/BM, 4FA/SSL/BM and 6FA/SSL/BM) was more than the PP, BM, 6FA/BM, and composites fabricated with 30 wt.% SSL fiber in PP (Mohanty et al. 2004; Jarukumjorn and Suppakarn 2009) (Maurya et al. 2021). Hybrid composite 2FA/SSL/BM, 4FA/SSL/BM and 6FA/SSL/BM showed 10.45%, 21.92% and 30.54%, increments in the tensile strength and 40.96%, 52.30%, and 45.12% increase in tensile modulus compared to pristine PP. This increase in tensile strength and modulus was possible due to the excellent dispersion of FA in the hybrid composite which supported an effective load transfer as previously reported by Sumesh (Sumesh et al. 2020), Gogoi (Gogoi et al. 2019a, c) and Khandelwal (Khandelwal and Rhee 2020)(Díez-Pascual and Naffakh 2013). Along with this, strong interfacial adhesion between alkali-silane treated SSL fiber and base matrix leads to good bonding at their interface (Panaitescu et al. 2019). The SSL fiber and base matrix interphase possible reactions could be esterification, hydrogen bonding, and polyamide (NH–CO) formation. The combined effect of both nano FA filler and treated SSL fiber ensures a high strength to the composite. Hence, a positive hybridization has been observed for the case as mentioned earlier. It is worth noting that treatment

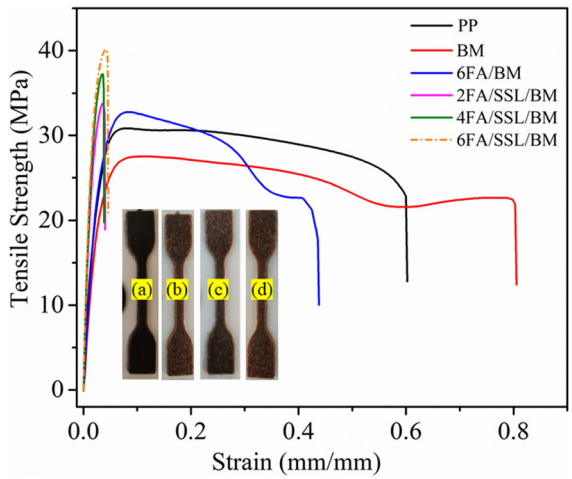

Fig. 2 Tensile stress vs. strain curve for hybrid composites and tensile specimen of **a** 6FA/BM **b** 2FA/SSL/BM **c** 4FA/SSL/BM **d** 6FA/SSL/BM

with 6% C-tab surfactant during ball milling provides the composite with most significant tensile property. This increase in the tensile property was due to the nanofiller's homogeneous mixing within the hybrid composite. As cationic surfactant percentage increases, the nanofiller's expected agglomeration ultimately decreases due to the repulsion between them.

Furthermore, inorganic FA fills the meso and micro voids in the matrix, ensuring good packing of the composites. Among all the hybrid composites, 6FA/SSL/BM demonstrated the highest tensile strength (40 ± 1.12 MPa) and modulus (1.50 ± 0.06 GPa). Positive hybridization was evident on the tensile properties due to the improved interfacial interaction and good dispersion of FA fillers. Better interfacial interaction and dispersion were achieved by the presence of MA-g-SEBS and C-tab treatment of the FA.

Micromechanics of the composites

Micromechanics of the composites and hybrid composites has been explained by comparing experimentally calculated data to the theoretical models proposed by different researchers. It is evident from Table 2 that for the particulate composite *eff*-BM, the rule of mixture (upper bound), inverse rule of mixture (lower bound) and Ishai and Cohen (lower bound) model give the value of the tensile modulus closest to the experimental one (which is 754 MPa shown by 6FA/BM filled with 5 wt.% FA). Other models (Counto, Ishai and Cohen (upper bound)) fail to give the exact result or do not come even nearby. Einstein, Guth and Mooney's equations predict value close to ~ 800 MPa but still was far away from the experimental value. Rule of mixture (upper bound) and inverse rule of mixture (lower bound) work on a principle of iso-stress and iso-strain criteria, and overall stress and strain carried by the composite is the sum of stress and strain carried by each FA and BM respectively (Tan et al. 2016). A homogeneous stress transfer and interfacial adhesion for a cubical reinforcement in a cubic matrix was presumed by Ishai and cohen (lower bound). In the current work, e*ff*-BM might have resembled these models and at lower concentration (5 wt.%) of FA, fillers were perfectly dispersed and interacted with the BM. Also, it is expected that reduced particle size of the FA will provide larger surface area for interaction with the base matrix and offering homogeneous distribution of stress.

Table 2 Description of estimates of modulus of composite using experimental and theoretical calculations

Experimental data	E (MPa) ± S.E
6FA/BM (*eff*-BM)	754 ± 15
2FA/SSL/BM (hybrid composite)	1423 ± 35
4FA/SSL/BM (hybrid composite)	1538 ± 30
6FA/SSL/BM (hybrid composite)	1465 ± 60
Empirical models for *eff*-BM	**$E_{eff\text{-}BM}$ (MPa) ± S.E**
Rule of mixture	**776 ± 13**
Inverse rule of mixture	**748 ± 08**
Ishai and Cohen (upper bound)	1498 ± 15
Ishai and Cohen (lower bound)	**752 ± 14**
Einstein equation	830 ± 21
Guth	819 ± 23
Counto	588 ± 14
Mooneys	817 ± 15
Combined empirical model for hybrid composites	**E_{Hybrid} (MPa)**
Rule of mixture + Rule of mixture	1804 ± 06
Rule of mixture + Inverse rule of mixture	1029 ± 19
Rule of mixture + Halpin Tsai	**1536 ± 08**
Inverse rule of mixture + Rule of mixture	**1785 ± 17**
Inverse rule of mixture + Inverse rule of mixture	1063 ± 28
Inverse rule of mixture + Halpin Tsai	**1482 ± 12**
Ishai and Cohen (lower bound) + Rule of mixture	1789 ± 14
Ishai and Cohen (lower bound) + Inverse rule of mixture	1036 ± 07
Ishai and Cohen (lower bound) + Halpin Tsai	2990 ± 25

E: experimentally obtained tensile modulus of composites, $\boldsymbol{E_{eff\text{-}BM}}$: theoretical tensile modulus of BM filled with 5 wt.% FA, and $\boldsymbol{E_{Hybrid}}$: theoretical tensile modulus of hybrid composites evaluated from combined empirical models.

The following models: Rule of mixture (upper bound), Inverse rule of mixture (lower bound) and Ishai and Cohen (lower bound), which predicted modulus for the particulate composite near to experimental value were considered further for the analysis of the hybrid composite. For the evaluation of tensile modulus of hybrid composite, the above models in combination with themselves or with Halpin–Tsai

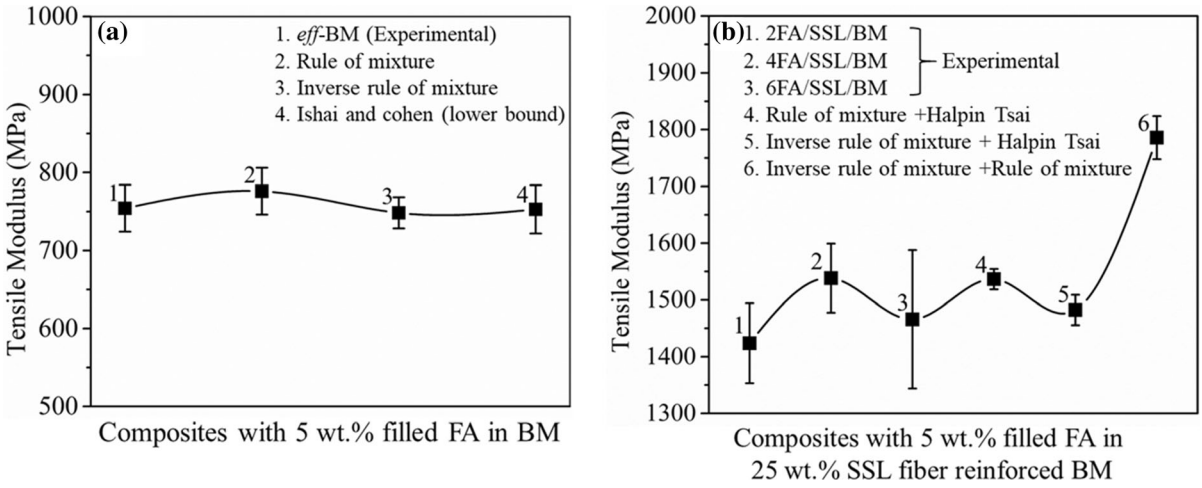

Fig. 3 A comparative study between experimental versus theoretical tensile modulus estimates **a** 5 wt.% FA reinforced BM composite **b** 5 wt.% FA hybridized sisal fiber reinforced composites

model (exclusively for fiber reinforced composite) were used and results presented in Table 2. As can be observed from the Table, the following combination of empirical models gave the closest value of tensile modulus to that of experimental data (1424–1530 MPa): Inverse rule of mixture + Halpin Tsai (1482 MPa), Rule of mixture + Halpin Tsai (1536 MPa) and Inverse rule of mixture + Rule of mixture (1785 MPa). Matching of the estimates of modulus from models with real-time prepared composite data strongly and the basic model assumptions confirms the better interfacial adhesion of the filler FA and reinforcing sisal fiber to the base matrix. A comparative bar diagram for experimental versus theoretical values for both 5 wt.% FA reinforced BM and 5 wt.% FA hybridized sisal fiber-reinforced composites has been given in Fig. 3a and b, respectively.

Flexural strength

Figure 4 shows the flexural behavior of PP, BM, and all the composites in the stress versus strain curve. Interestingly, like tensile properties, all the composites follow a similar trend for flexural strength and modulus. The flexural properties of hybrid composites 2FA/SSL/BM, 4FA/SSL/BM, and 6FA/SSL/BM improved significantly compared to pristine PP. Hybrid composites 2FA/SSL/BM, 4FA/SSL/BM and 6FA/SSL/BM showed an increment of ∼ 34%, ∼ 44%, and ∼ 48% for flexural strength, respectively

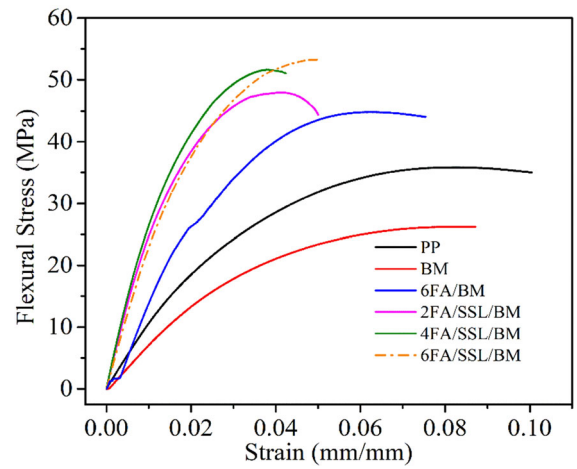

Fig. 4 Flexural strength versus flexural strain for hybrid composites

(Table 3). This increment was exhibited because of the effective load transference from matrix to reinforcement as a result of strong ester, hydrogen, and polyamide linkage formation between SSL fiber and BM, along with excellent dispersion of nanostructured C-tab FA. It was also expected nano FA must have reduced the gap at the interface of reinforcing SSL fiber and matrix. Contrarily, although 30 wt.% SSL fiber-reinforced composite (Maurya et al. 2021) and composite 6FA/BM showed flexural properties better than pristine PP, these were still less than all the hybrid composites fabricated in this study. 6FA/SSL/BM of all the composites exhibited the highest flexural

Table 3 PP, BM and composite's flexural and notched impact strength estimates

Sample	Flexural strength (MPa) ± S.E	Flexural modulus (GPa) ± S.E	Notched impact strength (kJ/m^2) ± S.E
PP	35.86 ± 0.09	1.00 ± 0.01	0.63 ± 0.02
BM	26.24 ± 0.06	0.73 ± 0.03	1.81 ± 0.08
6FA/BM	44.78 ± 0.07	1.54 ± 0.04	1.09 ± 0.07
2FA/SSL/BM	48.05 ± 0.05	2.30 ± 0.06	0.80 ± 0.04
4FA/SSL/BM	51.63 ± 0.08	2.50 ± 0.07	0.77 ± 0.06
6FA/SSL/BM	53.27 ± 0.10	2.5 ± 0.02	0.75 ± 0.03

strength (53 MPa) and modulus (2.5 GPa), respectively, with 6FA/BM showed the lowest flexural strength of 45 MPa and flexural modulus of 1.54 GPA. The trend of tensile properties was also observed for the flexural properties depicting a positive hybridization effect.

Flexural properties of all the hybrid composites reported better flexural performance compared to PP, BM, 6FA/BM, and 30 wt.% reinforced sisal fiber composite to the BM (Maurya et al. 2021).

A strong adhesion/interaction at the interface SSL fiber and BM and the inclusion of nanostructured FA leads to better load transfer. Additionally, a good dispersion of FA and gap reduction between interfaces of SSL fiber and BM must have played an important role in enhancing the load transfer from BM to SSL fiber as also observed earlier (Khandelwal and Rhee 2020; Sumesh et al. 2020).

FA treatment with low C-tab wt.% may have let the fillers to remain in a state of agglomeration, and hence, did not effectively help in increasing flexural properties (Satapathy and Kothapalli 2018).

Notched impact strength

Table 3 displays the notched Izod impact strength of PP, BM, and all the hybrid composites. Noticeably, an improved impact strength of all the composites was observed compared to neat PP. Reinforcing BM with natural fiber leads to reduced impact strengths of 2FA/SSL/BM, 4FA/SSL/BM, and 6FA/SSL/BM compared to 6FA/BM. This is in agreement with some literature reports which state that the reinforcement of stiff fiber to the polymer reduces the impact strength of the composites (Nourbakhsh et al. 2008)(Liu et al. 2009). However, these composites still reported better impact properties compared to 30 wt.% reinforced SSL/PP (0.58 kJ/m^2) composites. A significant improvement in the impact properties of 6FA/BM and hybrid composites 2FA/SSL/BM, 4FA/SSL/BM, and 6FA/SSL/BM of 73%, 26.98%, 22.22%, and 19.04% respectively over and above those of PP exhibited due to the replacement of PP with a relatively tougher BM. This pre-toughening of PP with MA-g-SEBS and SEBS before forming hybrid composites must have enhanced impact properties. Thus, the positive effect of MA-g-SEBS and SEBS incorporation into the PP on impact strength is quite evident.

Morphology

Figure 5a to c depicts the FE-SEM images of FA; high energy ball milled FA and hybrid composite, respectively. FESEM has confirmed the size of FA to be greater than 100 μm. However, the pristine FA fillers were ball milled in a planetary ball mill, and the size was reduced to least size of 400 nm, which can be confirmed from Fig. 5b.

Composite fabricated by reinforcing sisal fiber, nano range FA, and the base matrix has also been investigated. Figure 5c demonstrate the FE-SEM descriptions of the broken tensile specimen of the composite 4FA/SSL/BM. It has been observed that sisal fibers and FA are deeply embedded in the base matrix, and fibers are fully covered and wetted with polymers. There is no apparent voids or gap observed between the base matrix and fiber. The orientation of fibers inside the matrix is significant and, they appear uniformly distributed at all corners of the matrix. Good fiber and polymer interaction are a consequence of successful bonding at the interface of SSL fiber, FA, and base matrix. Sisal fiber and FA are fully adhered from the polymer matrix and confirm the composite.

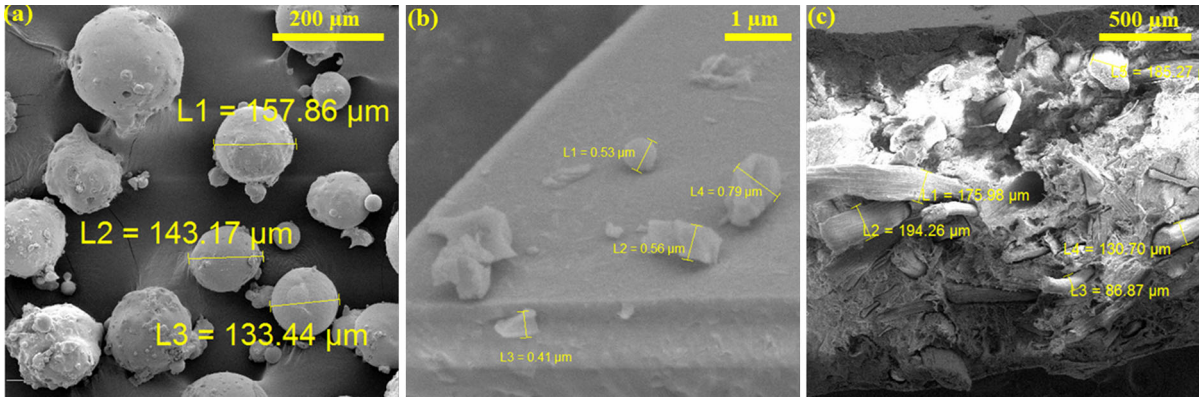

Fig. 5 FESEM images of **a** Pristine FA **b** High energy ball milled FA **c** hybrid composite

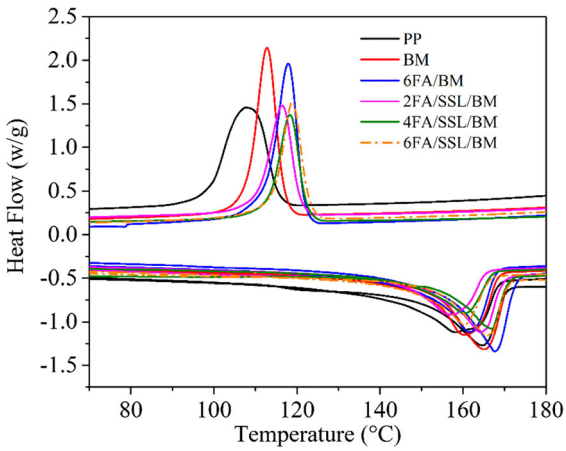

Fig. 6 Illustration of the thermogram of the PP, BM, composite 6FA/BM, 2FA/SSL/BM, 4FA/SSL/BM and 6FA/SSL/BM composites

Table 4 Estimates of crystallization and melting temperature, melting enthalpy and percentage crystallinity of pristine PP, base matrix and fabricated composites

Samples	T_c (°C)	T_m (°C)	ΔH (J/g)	% Crystallinity
PP	107.80	164.81	146.73	70.20
BM	112.77	165.13	90.249	43.18
6FA/BM	117.91	167.65	128.30	61.24
2FA/SSL/BM	116.47	164.23	147.57	70.60
4FA/SSL/BM	118.32	166.62	148.87	71.22
6FA/SSL/BM	118.91	165.70	145.37	69.55

DSC

Thermograms for the pristine PP, BM, and different composites have been depicted in Fig. 6. Endothermic and exothermic peaks of the curves correspond to the melting and crystallization temperature of the samples. Different parameters of PP, BM, and composites, including melting point (T_m), crystallization temperature (T_c) and melting enthalpy (ΔH) have been reported in Table 4.

Sengupta et al. (Sengupta et al. 2013a) reported different crystallographic phases of semi crystalline PP i.e. α-monoclinic phase, β-pseudohexagonal phase and γ-orthorhombic phase. The α-monoclinic phase of the PP is thermodynamically most stable form among all three phases. Melting peak (from second heating) of the PP observed at 164.81 °C, also reported earlier by Gogoi (Gogoi et al. 2019a) corresponds to the α-monoclinic crystal melting. A resemblance of the T_m of the composites with that of PP shows insignificant effect of the incorporating fillers on the melting behavior. There was negligible change in the melting point (165.13 °C) of the BM. However, composites 6FA/BM, 2FA/SSL/BM, 4FA/SSL/BM and 6FA/SSL/BM exhibited a melting point of 167.65 °C, 164.23 °C, 166.62 °C and 165.70 °C. The 2–3 °C shifting in the exothermic curve or crystallization temperature in all the composites may be due to the heterogeneous nucleating effect of the C-tab treated FA and SSL fiber which might have accelerated the crystallization rate at higher temperature (Gogoi et al. 2019a). It has also been worth mentioning that C-tab-FA incorporated composite shown the highest accelerated nucleating effect in comparison to 2FA/SSL/

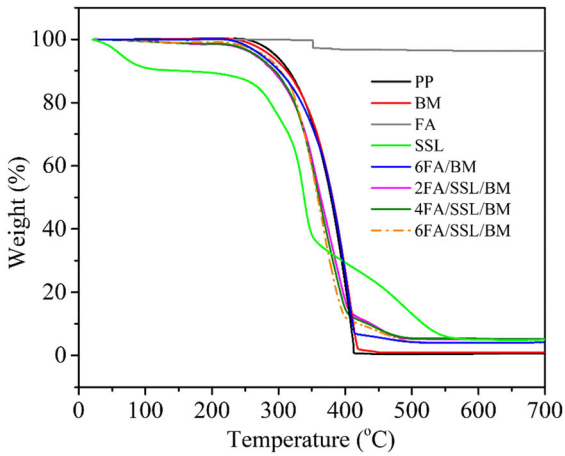

Fig. 7 Illustration of TGA for FA, SSL, PP, BM, and different composites

BM, 4FA/SSL/BM, and 6FA/SSL/BM that might be attributed to the smallest particle size of the FA.

Percentage crystallinity of the PP, BM and fabricated composites has been depicted in the Table 4. PP showed a crystallinity of 70.20% similar to reported values in literature (Jia and Raabe 2008). Based on expectations that incorporation of amorphous elastomer will lead to a decrease in the PP's crystalline percentage, the base matrix which contains 10% SEBS and 5% SEBS-MA used for the composites showed 43.18% crystallinity. Composites 6FA/BM, 2FA/SSL/BM, 4FA/SSL/BM and 6FA/SSL/BM exhibited a crystallinity of 61.24%, 70.60, 71.22% and 69.55% respectively, which is higher than the base matrix BM and near to PP. The increase in the crystallinity percentage of the composites compared to base matrix may be attributed to the FA fillers' nucleating effect, as discussed earlier. Such a situation of increase in crystallinity due to the incorporation of inorganic filler and short natural and glass fibers has also been reported by Gogoi et al.(Gogoi et al. 2019a).

Thermogravimetric analysis

The TGA curve of SSL fiber, FA, PP, BM, 6FA/BM, 2FA/SSL/BM, 4FA/SSL/BM and 6FA/SSL/BM are shown in Fig. 7. Temperatures of degradation at different weight % (5%, 50%, 75% and maximum loss) of SSL fiber, FA, PP, BM, 6FA/BM, 2FA/SSL/BM, 4FA/SSL/BM and 6FA/SSL/BM, represented by T_i, T_{50}, T_{75}, and T_{max}, have been reported in Table 5.

Table 5 shows that the lowest degradation temperature (T_i) was possessed by SSL fiber, and up to 100 °C it releases volatiles and moisture. A three-step degradation route was followed by SSL fiber. Initiation of degradation (T_i) of SSL fiber starts at 63 °C in the form of moistures and volatiles with final degradation (T_{max}) at 545 °C. Additionally, degradation of 50 and 75 wt.% loss of SSL fiber takes place at 338.19 °C and 431.80 °C. It was expected that degradation of cellulose (325–360 °C), depolymerization of hemicellulose (325–360 °C) and sample failure (425–460 °C) must have been completed in the mentioned temperature range (Gupta et al. 2012; Alam et al. 2014). Likewise, PP being hydrophobic in nature, shows one step degradation process (350–450 °C). Percentage weight loss such as T_i, T_{50}, T_{75}, and T_{max} has been reported at 295 °C, 378.66 °C, 398.23 °C, and 413 °C, respectively. The

Table 5 Degradation temperatures of SSL fiber, FA, PP, BM, and composites at different wt.% loss

Sample	T_i (°C)	T_{50} (°C)	T_{75} (°C)	$T_{max.}$ (°C)
Sisal (Maurya et al. 2021)	63.44	338.19	431.80	545.00
FA	512.14	NA	NA	NA
PP	295.01	378.66	398.23	413.38
BM	287.50	380.98	401.56	419.46
6FA/BM	274.33	379.78	400.83	415.12
2FA/SSL/BM	263.69	332.72	363.27	408.44
4FA/SSL/BM	266.23	332.08	360.53	404.96
6FA/SSL/BM	277.47	333.21	358.47	401.71

T_i: initial degradation temperature at 5% wt. loss, T_{50}: temperature at 50% wt. loss, T_{75}: temperature at 75% wt. loss, T_{max}: degradation temperature at maximum wt. loss

weight loss process of PP at lower temperature was prolonged while above 350 °C it degrades very rapidly and leaves a residue of 0.66% at 413 °C. FA being burnt waste and inert did not exhibit any significant change in weight loss upon heating except the loss of a small quantity of volatiles. Interestingly, the increment in the thermal stability of the composites has been exhibited due to the addition of FA. Among all the composites, 6FA/BM, reinforced with 5 wt.% FA possessed the highest temperature of degradation. However, the inclusion of SSL fiber to the hybrid composites decreases their degradation temperature, especially at T_{50} and T_{75} (Maurya et al. 2021). All the hybrid composites 2FA/SSL/BM, 4FA/SSL/BM, and 6FA/SSL/BM exhibited T_{50} and T_{75} degradation temperature lower than that of 6FA/BM composite. Complete degradation of SSL fiber, FA, PP, BM, and all the composites takes place < 550 °C. A residue of 5.10%, 97%, 0.66% and 0.70% was left for sisal fiber, FA, PP, and BM at $\sim$ 800 °C. Composites 6FA/BM, 2FA/SSL/BM, 4FA/SSL/BM, and 6FA/SSL/BM have not released volatile matters like SSL. Residual mass at 800 °C for 6FA/BM, 2FA/SSL/BM, 4FA/SSL/BM, and 6FA/SSL/BM composites was around 4.05%, 5.16%, 5.40%, and 4.07%, respectively, which laid betwwen PP and FA.

Conclusions and future direction

FA hybridized SSL fiber reinforced PP composites with improved mechanical properties compared to PP were fabricated successfully. The major finding from this research was the positive hybridization effect of FA, which was improved for tensile and flexural properties compared to the data reported in our previous study. The highest tensile strength and modulus of 40.12 MPa and 1.47 GPa were reported for 6FA/SSL/BM. This significant improvement was more than 30.09% and 2.08% respectively compared to the same wt.% of FA and SSL fiber-reinforced BM, reported by us earlier. Likewise, flexural strength (53.24 MPa) and modulus (2.50 GPa) of 6FA/SSL/BM reported an increment of 35.40% and 66.66% compared to the equivalent composite (5 wt.% of FA and 25 wt.% of SSL) reported in our previous study. High energy ball milling and C-tab treatment of nanostructured FA have most probably added this positive effect to the mechanical properties. Tensile and flexural properties of the composites were also improved upon increasing the treatment percentage from 2 to 6% of the FA with C-tab surfactant. However, there was a slight decrease in tensile modulus of 6FA/SSL/BM compared to 4FA/SSL/BM. The resemblance of the experimentally calculated modulus value to the predicted modulus from a combination of the Inverse rule of mixture and rule of mixture with Halpin–Tsai confirms that the principal of iso-stress and iso strain is working for hybrid composites. 6FA/BM and 6FA/SSL/BM exhibited impact strength of 1.09 and 0.75 kJ/m^2 which were respectively highest and lowest among all the composite formulations and also in comparison to PP (0.63 kJ/m^2) these strength values were higher.

Furthermore, the addition of stiff SSL fiber to the hybrid composites decreased impact properties but still was better than PP. The stiffening nature of SSL fiber was compensated by the addition of SEBS and MA-g-SEBS to the BM. FE-SEM study confirmed the excellent dispersion and wetting of fiber and FA particles in the base matrix BM). A shifting of 2–3 °C in the exothermic curve or crystallization temperature for all the composites has been observed. Composites 6FA/BM, 2FA/SSL/BM, 4FA/SSL/BM, and 6FA/SSL/BM exhibited a crystallinity of 61.24%, 70.60, 71.22%, and 69.55%, respectively, which was higher than the base matrix BM and near to PP. Although the addition of FA increased the thermal stability of composites, the inclusion of SSL fiber in the composite system decreased their degradation temperature, especially at T_{50} and T_{75}. Hence, as a result, 2FA/SSL/BM, 4FA/SSL/BM, and 6FA/SSL/BM exhibited T_{50} and T_{75} degradation temperatures lower than that of 6FA/BM composite.

The above conclusions confirm that a combination of both nano-structured FA and SSL fiber reinforced in BM can be used to make injection molded parts with high tensile, flexural, and impact properties of the different automobile industries. Using these composites instead of virgin polymers will reduce cost and save the environment in terms of value-added utilization of waste industrial by-products. Nanostructured FA enhanced the mechanical properties of the natural fiber reinforced polymer composite. Replacing inorganic fillers used by the auto industry with high-energy ball-milled FA could be a logical step in managing waste. Natural fiber-reinforced polymer composites tend to absorb water and possess low

thermal degradation; however, the addition of nanostructured FA mitigates water absorption by filling meso and micropores at the interfaces and increases thermal stability.

Acknowledgements All the authors of this work acknowledge IIT Roorkee for providing technical support. First and second author would also like to acknowledge the Ministry of Human Resources and Development (MHRD) for providing monthly research fellowship.

Declarations

Conflict of interest All the authors of the current work agreed, read and approved the manuscript. The current manuscript in part or full has not been submitted anywhere. The authors have no conflicts of interest to declare that are relevant to the content of this article.

Ethical approval This study does not involve any animal/human testing for completing the research.

Ethical standard Data and figures reported in the manuscript were as per scientific community standard.

References

Abdal-Hay A, Suardana NPG, Choi KS, Lim JK (2012) Effect of diameters and alkali treatment on the tensile properties of date palm fiber reinforced epoxy composites. Int J Precis Eng Manuf 13(7):1199–1206. https://doi.org/10.1007/s12541-012-0159-3

Abral H, Kadriadi D, Rodianus A et al (2014) Mechanical properties of water hyacinth fibers–polyester composites before and after immersion in water. Mater Des 58:125–129

AL-Oqla FM (2021) Performance trends and deteriorations of lignocellulosic grape fiber/polyethylene biocomposites under harsh environment for enhanced sustainable biomaterials. Cellulose. https://doi.org/10.1007/s10570-020-03649-x

AL-Oqla FM, Hayajneh MT (2020) A hierarchy weighting preferences model to optimise green composite characteristics for better sustainable bio-products. Int J Sustain Eng. https://doi.org/10.1080/19397038.2020.1822951

Alam T, Gupta MK, Srivastava RK, Singh H (2014) Thermal Characterization and fracture toughness of sisal fiber reinforced polymer composite. Int J Sci Eng Technol 3:1071–1073

Black MJ, Whittaker C, Hosseini SA et al (2011) Life Cycle Assessment and sustainability methodologies for assessing industrial crops, processes and end products. Ind Crops Prod 34:1332–1339. https://doi.org/10.1016/j.indcrop.2010.12.002

Díez-Pascual AM, Naffakh M (2013) Polypropylene/glass fiber hierarchical composites incorporating inorganic fullerene-like nanoparticles for advanced technological applications. ACS Appl Mater Interfaces 5:9691–9700. https://doi.org/10.1021/am402750t

Faruk O, Bledzki AK, Fink H, Sain M (2012) Progress in polymer science biocomposites reinforced with natural fibers: 2000–2010. Prog Polym Sci 37:1552–1596. https://doi.org/10.1016/j.progpolymsci.2012.04.003

Filho AS, Parveen S, Rana S et al (2021) Micro-structure and mechanical properties of microcrystalline cellulose-sisal fiber reinforced cementitious composites developed using cetyltrimethylammonium bromide as the dispersing agent. Cellulose. https://doi.org/10.1007/s10570-020-03641-5

Gadioli R, Morais J (2014) The role of lignin in polypropylene composites with semi-bleached cellulose fibers: mechanical properties and its activity as antioxidant. Polymer Degrad Stab 108:23–34

Gogoi R, Kumar N, Mireja S et al (2019a) Effect of Hollow glass microspheres on the morphology, rheology and crystallinity of short bamboo fiber-reinforced hybrid polypropylene composite. JOM 71:548–558. https://doi.org/10.1007/s11837-018-3268-3

Gogoi R, Kumar N, Mireja S et al (2019b) Natural fibre based hybrid polypropylene composites: an insight into thermal properties. In: ICCM international conferences on composite materials, Melbourne, Australia

Gogoi R, Manik G, Arun B (2019c) High specific strength hybrid polypropylene composites using carbon fibre and hollow glass microspheres: development, characterization and comparison with empirical models. Compos Part B Eng 173:106875. https://doi.org/10.1016/j.compositesb.2019.05.086

Gupta AK, Biswal M, Mohanty S, Nayak SK (2012) Mechanical, thermal degradation, and flammability studies on surface modified sisal fiber reinforced recycled polypropylene composites. Adv Mech Eng 2012:13. https://doi.org/10.1155/2012/418031

Hamidon MH, Sultan MTH, Ariffin AH, Shah AUM (2019) Effects of fibre treatment on mechanical properties of kenaf fibre reinforced composites: a review. J Mater Res Technol 8:3327–3337

Jarukumjorn K, Suppakarn N (2009) Effect of glass fiber hybridization on properties of sisal fiber-polypropylene composites. Compos Part B Eng 40:623–627. https://doi.org/10.1016/j.compositesb.2009.04.007

Jia J, Raabe D (2008) Crystallinity and crystallographic texture in isotactic polypropylene during deformation and heating. arXiv preprint. arXiv:0811.2412

Joseph S, Bambola VA, Sherhtukade VV, Mahanwar PA (2011) Effect of flyash content, particle size of flyash, and type of silane coupling agents on the properties of recycled poly(ethylene terephthalate)/flyash composites. J Appl Polym Sci 119:201–208. https://doi.org/10.1002/app.32449

Khandelwal S, Rhee KY (2020) Recent advances in basalt-fiber-reinforced composites: tailoring the fiber-matrix interface. Compos Part B Eng 192:108011. https://doi.org/10.1016/j.compositesb.2020.108011

Koohestani B, Mokhtari AKDP, Darezereshki EYE (2019) Comparison of different natural fiber treatments: a literature review. Int J Environ Sci Technol 16:629–642. https://doi.org/10.1007/s13762-018-1890-9

Kumar N, Mireja S, Khandelwal V et al (2017) Light-weight high-strength hollow glass microspheres and bamboo fiber based hybrid polypropylene composite: a strength analysis and morphological study. Compos Part B Eng 109:277–285. https://doi.org/10.1016/j.compositesb.2016.10.052

Liu H, Wu Q, Han G et al (2008) Compatibilizing and toughening bamboo flour-filled HDPE composites: mechanical properties and morphologies. Compos Part A Appl Sci Manuf 39:1891–1900. https://doi.org/10.1016/j.compositesa.2008.09.011

Liu H, Wu Q, Zhang Q (2009) Preparation and properties of banana fiber-reinforced composites based on high density polyethylene (HDPE)/Nylon-6 blends. Bioresour Technol 100:6088–6097. https://doi.org/10.1016/j.biortech.2009.05.076

Maurya AK, Gogoi R, Manik G (2021) Study of the moisture mitigation and toughening effect of fly-ash particles on sisal fiber-reinforced hybrid polypropylene composites. J Polym Environ. https://doi.org/10.1007/s10924-021-02043-3

Mohanty S, Verma SK, Nayak SK, Tripathy SS (2004) Influence of fiber treatment on the performance of sisal-polypropylene composites. J Appl Polym Sci 94:1336–1345. https://doi.org/10.1002/app.21161

Naveen J, Jawaid M, Amuthakkannan P, Chandrasekar M (2018) Mechanical and physical properties of sisal and hybrid sisal fiber-reinforced polymer composites. Mechanical and physical testing of biocomposites, fibre-reinforced composites and hybrid composites. Elsevier, Amsterdam, pp 427–440

Nourbakhsh A, Kokta BV, Ashori A, Jahan-Latibari A (2008) Effect of a novel coupling agent, polybutadiene isocyanate, on mechanical properties of wood-fiber polypropylene composites. J Reinf Plast Compos 27:1679–1687

Panaitescu DM, Vuluga Z, Sanporean CG et al (2019) High flow polypropylene/SEBS composites reinforced with differently treated hemp fibers for injection molded parts. Compos Part B Eng 174:107062. https://doi.org/10.1016/j.compositesb.2019.107062

Sanjay MR, Arpitha GR, Naik LL et al (2016) Applications of natural fibers and its composites: an overview. Nat Resour 07:108–114. https://doi.org/10.4236/nr.2016.73011

Sanjay MR, Madhu P, Jawaid M et al (2018) Characterization and properties of natural fiber polymer composites: a comprehensive review. J Clean Prod 172:566–581

Sanjay MR, Siengchin S (2019) Lightweight Natural Fiber Composites. J Appl Agric Sci Technol 3:178. https://doi.org/10.32530/jaast.v3i2.108

Satapathy S, Kothapalli RVS (2018) Mechanical, dynamic mechanical and thermal properties of banana fiber/recycled high density polyethylene biocomposites filled with flyash cenospheres. J Polym Environ 26:200–213. https://doi.org/10.1007/s10924-017-0938-0

Sengupta S, Maity P, Ray D, Mukhopadhyay A (2013a) Stearic acid as coupling agent in fly ash reinforced recycled polypropylene matrix composites: structural, mechanical, and thermal characterizations. J Appl Polym Sci 130:1996–2004. https://doi.org/10.1002/app.39413

Sengupta S, Pal K, Ray D et al (2011) Furfuryl palmitate coated fly ash used as filler in recycled polypropylene matrix composites. Compos Part B Eng 42(7):1834–1839

Sengupta S, Ray D, Mukhopadhyay A (2013b) Sustainable materials: value-added composites from recycled polypropylene and fly ash using a green coupling agent. ACS Sustain Chem Eng 1:574–584. https://doi.org/10.1021/sc3000948

Senthilkumar K, Saba N, Rajini N et al (2018) Mechanical properties evaluation of sisal fibre reinforced polymer composites: a review. Constr Build Mater 174:713–729

Sumesh KR, Kavimani V, Rajeshkumar G et al (2020) An investigation into the mechanical and wear characteristics of hybrid composites: influence of different types and content of biodegradable reinforcements. J Nat Fibers. https://doi.org/10.1080/15440478.2020.1821297

Surani D (2021) politechnika wrocławska wydział mechaniczny kierunek: mechanika i budowa maszyn praca dyplomowa inżynierska. Wrocław University of Science and Technology

Tan JF, Jia YJ, Li LX (2016) A series-parallel mixture model to predict the overall property of particle reinforced composites. Compos Struct 150:219–225. https://doi.org/10.1016/j.compstruct.2016.04.047